APPLICATION OF VORTICITY CONFINEMENT TO ROTORCRAFT FLOWS

Yonghu Wenren
Flow Analysis Inc.
Tullahoma, TN, USA

John Steinhoff
University of Tennessee Space Institute
Tullahoma, TN, USA

Francis Caradonna
Ames Research Center
Moffett Field, CA, USA

Abstract

The Vorticity Confinement (VC) method has been presented for rotorcraft flows. Although the basic ideas are somewhat different than conventional CFD, there is some commonality with a number of well-known computational methods, such as shock capturing.

The main goal of VC is to efficiently compute complex high Reynolds number incompressible flows, including blunt bodies with extensive separation and shed vortex filaments that convect over long distances. Almost all of the vortical regions in these flows are turbulent. This means that, for any feasible computation, they must be modeled. The remainder of the flows is irrotational and is defined once the vortical distributions are. Furthermore, these vortical regions are often very thin.

For these reasons, the basic approach of VC is to efficiently model these regions. The most efficient way to do this appears to be to develop model equations directly on the computational grid, rather than to first develop model partial differential equations (pde's) and then attempt to accurately discretize them in these very thin regions.

These goals are easily achieved in the large number of flows where the essential features of the main flow are not sensitive to the internal structure of thin vortical regions. Then, VC can easily be used to capture these regions over only a couple of grid cells and to propagate them, essentially as nonlinear solitary waves that "live" on the computational lattice. Flows with these features that are treatable with the present state of VC include many rotorcraft flows. These involve complex geometries that can be easily "immersed" in uniform Cartesian grids using VC. These flows also include vortex filaments which can convect, with no numerical spreading, even over arbitrarily long times, and which can merge automatically with no requirement for special logic.

Preliminary results, some of which are presented, suggest that very large computer savings can be achieved, even with the simplest form of VC.

1.Introduction

There are a number of features that make the computation of rotorcraft flows a very different and much more difficult problem compared to fixed-wing aircraft flows.

(1) The most obvious is the tip vortex. This vortex convects away from a conventional aircraft with little interaction and does not have to be treated accurately. For example, most CFD methods can be used for its treatment, in spite of the fact that they may dissipate it significantly. By contrast, the rotor tip vortex convects closely past the following blade and has a strong influence on the induced flow, and hence lift. Also, it may impinge on the blade, resulting in blade-vortex interaction (BVI) noise. If conventional CFD methods are used, on feasible grids, the dissipation will lead to inaccurate induced flow, and hence loading and BVI noise. Finally, unlike aircraft in cruise, the tip vortex is not steady, even in a coordinate system rotating with the rotor in hover. This is because of the influence of the body.

(2) The rotorcraft body, together with the tail rotor, is a much more complex configuration than an aircraft. Fitting a curvilinear grid to the surface is difficult and, for reasons stated below in (3), may not be necessary or even consistent with the treatment of the wake of the body.

(3) The rotorcraft is a blunt body, shedding a large, turbulent wake. It is very different from a streamlined airplane fuselage/wing, which has little separation in normal conditions. The larger scales in the turbulent wake may be computed with conventional CFD, but the effect of the smaller scales must be treated with an approximate model equation. This wake, together with the tip vortices, subjects the body to strongly fluctuating flow, very different from that of a cruising aircraft. These conditions, together

with the approximations in the turbulent wake, make it unlikely that a RANS type turbulent boundary layer (TBL) model can be tuned to give the highly accurate drag predictions desired in fixed wing aircraft. For these reasons, we feel that accurately fitting the body with a curvilinear grid and using a finely tuned TBL model may not be consistent with the coarse-grained treatment and level of approximation of the rest of the flow field: For example, the strong vortices in the wake are not fitted with a grid but are "immersed" in a smooth, Cartesian type. A consistent treatment of the body would also involve immersed surfaces, resulting in a much simpler geometry setup and flow configuration. This should give force predictions with no less accuracy than if a body fitted grid were used, because of the other approximations in the complex, turbulent flow.

(4) A final, but not so obvious, point involves the goal of the computation: Fixed wing aircrafts are designed to operate close to a design point, and a goal is often to minimize drag for that single condition, which requires high accuracy in the drag computation. By contrast, a rotorcraft is subject to a very wide range of flight conditions, and adequate performance over this range must be assured. This means that the emphasis should be on performing a very large number of more approximate computations for these conditions. These simulations could help avoid problems often seen in the flying prototypes, such as tail-shake in the Comanche and the disastrous vortex ring state in the V-22.

The points described above emphasize the need for a method quite different from aircraft CFD. A very large number of simulations is needed, where each should have an accuracy only commensurate with that of the turbulent wake, to be consistent and should be as simple and efficient as possible. Toward this goal, computing any unnecessary details should be avoided. These details will turn out to be the time averaged internal structure (IS) of the TBL, the IS of the small vortical scales in the turbulent wake (as in any LES) and also the IS of the tip vortex.

By avoiding the computation of these details, which in any case are turbulent, model dependant, and strongly subject to numerical effects, it will turn out that the effects on the large scales are still computed with consistent accuracy, and more accurate model-independent results would not be possible anyway because of the wake. In this way, a very large improvement in computational speed can be achieved.

In this paper, first, the basic method used, "Vorticity Confinement" (VC), will be briefly described. There are a number of papers that have more descriptions which will be referred to. Then, some previous results that are relevant to rotorcraft flows will be briefly reviewed. These include helicopter body flows that involve a Cartesian grid incompressible solver (SAGE). These previous results also include rotor flows that involve coupling the above solver to a surface fitted compressible solver ("TURNS") near the blades.

The goal of our current research involves development of a "minimal" solver that will have the same accuracy as the above coupled one but will be simpler and faster. The main approach here is to represent the rotor blades as lifting lines, which move through the same Cartesian grid as is used for the body. Then, the entire "inner" part of the flow (rotor/body) is computed on a simple uniform Cartesian grid (a coarser "outer" grid is used to extend the computational domain). Preliminary results of these efforts are presented, which demonstrate on the ability to adequately resolve the wake, even on a coarse, uniform grid.

2. Approach

The approach involves employing a new finite difference algorithm on a uniform Cartesian grid (or a small number of nested grids). This algorithm "captures" the small vortical scales and, effectively, results in a simple implicit model for them. The regions modeled, as stated, include tip vortex cores, boundary layers, and small scales in the blunt body wake, which are all turbulent and must be modeled in any case. In our approach, however, we do not formulate a model partial differential equation (PDE) and then attempt to discretize it on the grid. Instead, the modeling is directly on the grid. This allows the thin regions to be captured over only several grid cells in the cross section, as opposed to 10-20 to accurately solve a turbulent model PDE (even then, the result is, of course, only an approximation).

There are a number of requirements on these implicit models, including mass and (approximate) momentum conservation. For the boundary layer, these also include ensuring a correct total vorticity, by enforcing a zero velocity (no-slip) boundary condition. Then, when the layer separates, it will have the correct effect on the flow. This requires that the boundary layer, as well as the other small scales, remain small even when convected over long distances.

Some of these features stated above are similar to that of vortex lattice (panel) methods. However, in our method (Vorticity Confinement), the vortical features are not carried by markers but represented on a grid, as in conventional CFD. This gives the flexibility of the conventional CFD methods. An analogy could be made: comparing our method to vortex lattice method is like comparing shock

capturing that uses a smooth grid where shocks can automatically merge, etc., with shock fitting methods that require sets of markers to define each shock.

Both traditional methods have drawbacks and advantages for treating thin vortical regions: panel methods are economical, but, except for very simple cases, require complex logic – such as for vortex/body interaction, including separation, and vortex merging and reconnection. CFD methods are very flexible, as long as there is not much of grid adaptation, in that they allow any changes in topology of the vortical regions. However, they represent a very inefficient model of the thin vortical regions, requiring a number of thin grid cells and extensive grid adaptation, which is expensive since the real flows to be treated are unsteady.

The basic features of the method described in the next section, Vorticity Confinement, combine the advantages of both of the above traditional methods but avoid most of their disadvantages.

3. Vorticity Confinement

The original version of Vorticity Confinement ("VC1") has seen a number of uses (Refs. 1-27). This paper will concentrate on its use in rotorcraft aerodynamic computations. The basic features and formulation are described in this section: It consists, basically of a term added to the discretized momentum equations, which is non-zero only in vortical regions. Its use as a boundary layer model is quite simple and effective and results will be referred to. For rotor tip vortices it also has proven to be effective. Here, the fact that it closely conserves total momentum results from the rapid rotation of the vortex, since it is not written in an explicitly momentum conserving form. A preliminary computation (Ref. 9) involving coupling to the "TURNS" code has shown good agreement with experiment, and will be reviewed in this section. As explained in Sec. 2, a new simpler, more efficient use with lifting lines is currently being developed. Some preliminary results will be presented at the end of this section. Comparisons of the completed version with experiment will be reported in a subsequent paper.

A second version, "VC2", has recently been developed, which explicitly conserves momentum. This has been described in a number of recent papers (Refs. 14, 15, 20) and will not be discussed here. Rotor computations are currently being developed based on it. Preliminary results appear to give tip vortex trajectories close to those of VC1. These will also be reported in a subsequent paper.

Along with these rotor computations, uses of VC1 for flow over bodies "immersed" in a uniform Cartesian grid will be presented for validation. The rest of this section is close to Section 3 of Ref. (9), and is included for completeness.

3.1 Basic Concept The basic idea behind Vorticity Confinement is to develop a set of difference equations on a fixed grid (typically uniform Cartesian) that fulfill the above requirements. This implies that the equations must be an accurate discretization of the Euler pde's in the outer irrotational regions, but reduce to a set of *difference equations* (as opposed to finite difference approximations of pde's) in the vortical regions, where flow quantities vary by $O(1)$ over a few grid cells. Further, to allow separation, reattachment, merging, etc., the vortical structure cannot be specified. Instead, the structure must relax to the desired profile as it convects.

The above requirements mean that there should be two basic parameters in the method: a length scale and a time scale. These are directly related to the grid cell size and time step of the computation, i.e., the resulting vortical profile should be a few grid cells wide and the relaxation should take place over a small number of time steps. Of course, if relevant, more complex models (including, for example, boundary layer dynamics or long-term viscous spreading) can be implemented which would involve more parameters. These are currently being formulated for cases with separation from smooth surfaces.

Some of the basic ideas are demonstrated for the advection of thin pulses in 1-D in Ref. (2), where the pulses are essentially treated as discrete solitary waves which propagate indefinitely without changing shape.

3.2 Formulation The simplest formulation of Vorticity Confinement involves, for general unsteady incompressible flow, adding two terms to the discretized momentum conservation equations in a primitive variable formulation, which are similar to the diffusion and nonlinear anti-diffusion term for the advecting short pulse discussed in Ref. (2). These terms are inherently multidimensional and Galilean invariant, depend only on local variables and vanish outside the vortical regions.

The governing equations with the Vorticity Confinement terms are then a discretization of the following equations:

$$\nabla \cdot \vec{q} = 0$$

$$\partial_t \vec{q} = -(\vec{q} \cdot \nabla)\vec{q} - \nabla(P/\rho) + [\mu \nabla^2 \vec{q} - \varepsilon \vec{s}]$$

where $\vec{q}$ is the velocity vector, p pressure, and ρ, density, and the two terms in brackets are the confinement terms. The two numerical coefficients, ε and μ, control the size of the convecting vortical regions or vortical boundary layers and their relaxation rate to a quasi-steady shape.

There are many possible forms for the second Confinement term. The simplest one seems to be

$$\vec{s} = \hat{n} \times \vec{\omega}$$

where

$$\hat{n} = \frac{\nabla \eta}{|\nabla \eta|}$$

and the vorticity vector is given by

$$\vec{\omega} = \nabla \times \vec{q}$$

The scalar field, η, is defined in two ways:

$$\eta = \begin{cases} |\vec{\omega}| : & \text{"Field Confinement"} \\ |F| : & \text{"Surface Confinement"} \end{cases}$$

(F: distance from surface)

The simplest implementation of Vorticity Confinement, for convecting vortices, is called “Field Confinement”. A simple modification; “Surface Confinement”, for boundary layers, will be described in the next section.

For Field Confinement, the unit vector, $\hat{\eta}$, points towards the local centroid of the vortical region, and the confinement term serves to convect vorticity back towards the centroid as it diffuses away. This convection increases the diffusion term and a steady-state distribution automatically results when the two terms become balanced (for any reasonable values of μ and ε). Additional discussions of the formulation can be found in Refs. (1, 3, 4, 6, 14).

An important feature of the Vorticity Confinement method is that the extra terms are limited to the vortical regions: both the diffusion term and the confinement term vanish outside those regions. Another important feature concerns the total change induced by the correction in mass, vorticity and momentum, integrated over a cross section of a convecting vortex sheet or filament. It is shown in Refs. (1, 3, 4, 6, 14) that mass and vorticity are explicitly conserved and momentum is closely conserved. Extensions of the method, described below in Refs. (5,14,24), allow it to also explicitly conserve momentum. This has no observable effect on most results, except for cases involving long-term convection of vortices in a low velocity field. Then, the momentum conserving extension is easily implemented to ensure accurate trajectories.

In general, computed flows do not depend sensitively on the parameters ε and μ, for a range of values. Hence, the issues involved in setting them are similar to those involved in setting numerical parameters in other standard computational fluid dynamics schemes, such as artificial dissipation in many conventional compressible solvers which capture shocks. The main effect of varying ε and μ, within a range, is to vary the vortex core radius, which is approximately equal to μ/ε (Refs. 1, 6).

The reason for this lack of sensitivity is that, for example, if a vortex core is close to axisymmetric, the velocity outside the core is not sensitive to the vorticity distribution or core size, as long as the radius is kept small and prevented from becoming large due to numerical effects. This is a well-known property of axisymmetric, parallel vortices. It means that their mutual interaction will also be independent of the structure, as long as they are separated. Since merging, etc. takes place on convective time scales, this is also not sensitive (Refs. 1, 14). This lack of sensitivity to ε was also demonstrated for a rolling-up vortex sheet computation in Refs. (3, 6) where ε was varied by a factor of 4 and the result remained close to experiment, while for $\varepsilon = 0$ the result was much too diffusive. This was also shown in Ref. (8) for dynamic stall. Similar considerations apply to thin boundary layers. (This is analogous to the artificial shock thickness effects that depend on the dissipation parameter).

In addition to the solitary wave-like features of the vorticity distribution for free convecting vortices in 2D and 3D (convection with fixed shape), two studies, Refs. (1, 4), demonstrated the ability of convecting 3D vortex filaments, initially in the form of rings, to merge and reform. A comparison of these results (Ref. 1) with measurements from an experiment, published in Ref. (4), showed a very close agreement. This demonstrated that the basic computational concept of relaxing to a quasi-steady vortical state through the action of the diffusion and nonlinear terms automatically allows realistic vortex filament reconnection while at the same time preventing spreading due to numerical effects. This is true even though a coarse grid was used where the vortex cores were only ~3 grid cells in diameter. It has been shown numerically that vortical solutions to the discretized equations are qualitatively close to those predicted for the continuum ones, even though the

vortical regions are only a few cells thick. Roughly speaking, the confinement terms seem to be convecting discretization errors into the vortex center.

3.3 Solid Surface Modeling with Uniform Cartesian Grids The application of Vorticity Confinement to fixed vortex sheets representing solid surfaces in a non-conforming regular Cartesian grid with no-slip boundary conditions has been presented in Refs. (2, 9-12, 19, 23, 25). This represents a very simple, economical way to treat complex bodies since it does not require body conforming or adaptive grid generation and can use a fast Cartesian grid set-up and flow solver. The steps for this method are delineated below:

- The geometry of the body or free surface is specified in a conventional way - such as by the coordinates of a set of points on the surface.
- From this set of points, a smooth function is computed on each point of a regular Cartesian computational grid. The value of this function, $F(\vec{x})$, is the (signed) distance of the grid point to the defined surface. Thus, the "level set" of values of $\vec{x}$ such that $F(\vec{x}) = 0$ implicitly defines the surface over which the flow is to be solved. This *F = 0* surface can be complicated and even move according to dynamical equations.
- The flow over the *F = 0* surface is computed time-accurately in a sequence of time-steps. This involves confining vorticity to the (fixed) *F = 0* surface, as well as the convecting vortical regions.

3.4 Properties of Converged Solution At convergence, $\vec{q}$ is forced to zero inside the body. Since $\nabla \cdot \vec{q} = 0$ everywhere, there is then no flow through the body surface and vorticity is confined to thin regions on the body surface and thin regions which separate and convect with the flow. These regions are 2~3 grid cells thick, independent of the grid cell size *h* or number of grid points in the overall problem (in the fine-grid limit when h << radius of curvature). Further, since the computed velocity has zero divergence, if the separation locations are accurate, (as at edges or in regions of strong adverse pressure gradient), the computed velocity field will be at least first-order accurate in the grid cell size both away from convecting vortices and the body surface. The first-order error is due to the thickness of the computed vortical regions: simple perturbative corrections to bring the solution to second-order accuracy can be formulated within the framework of the method by considering the error as a displacement-thickness effect. This procedure should be simpler for many cases than resorting to the generation of a body conforming grid or adaptive high order refinement. However, for blunt body flows with separation the first order accuracy should be more consistent with the accuracy of the computation of the separating vorticity.

4. Results

4.1 Overset Grid Computation of Rotor/Wake Flow The rotor wake was computed for a two bladed case for which there is experimental data on the wake trajectory (Ref. 28). This rotor/wake system flow problem is solved by a simple overset procedure involving a Cartesian grid for the wake convection and a blade-fitted C-grid for the rotor flow near the blades. The inner C-grid region used the compressible, "Euler/Navier-Stokes Solver, TURNS (Ref. 29), to obtain the blade flow and circulation distribution. The background Cartesian grid uses an incompressible solver with Vorticity Confinement. The action of the inner solver is to generate the rotor lift distribution in response to the inflow generated by the convected wake. The two grids exchange information by interpolation. The inner C-grid flow is interpolated onto the Cartesian grid while the boundary values on the outer surface of the C-grid are interpolated from the Cartesian grid, according to the local characteristic directions.

Computed vorticity contours (with a lower limit of 25% of maximum vorticity magnitude) of the shed wake of a two-bladed rotor are shown in Ref. (30) These contours are not shown here but are almost identical to those of our present studies, discussed below and shown in Figs. (15, 16). The important features are that the vortex cores are captured in only a few grid cells. It is seen that the rotor tip vortex maintains its identity and that it behaves appropriately, showing correct radial contraction. Comparisons of measured and computed tip vortex trajectories are quite good, and it is known that this is a prerequisite to obtaining the correct loading.

It should be mentioned that the VC1 Vorticity Confinement method was used for this computation, without modification or adjustable, case dependent parameters.

4.2 Computation of Fuselage Flow The first objective for this computation was to quantify the model used for treating body surfaces in Cartesian grids: in particular, the ability to accurately predict surface pressure distributions. First, predicted flow was compared to the exact solution for a Cauchy Riemann flow about a two-dimensional circular cylinder. This is reported in Ref. (30). Then, the computation of convecting viscous flow over an ellipsoid was computed and compared with

experiment. This is reported in Refs. (13, 23). After this, computations of flow over a test case helicopter fuselage were done and predicted surface pressures at various streamwise stations compared to wind tunnel data. Then, the computation of flow over a complete Apache helicopter, including rotor, fuselage and wake was computed. Flow around a circular cylinder was also computed using both VC1 and VC2. Finally, the effects of vorticity shed from the pylon on a Comanche helicopter were computed and compared (by Ted Meadowcraft Ref. (31)) to measured values.

4.2.1 Computation of Flow over ROBIN Fuselage The new extrapolation procedure was evaluated for flow about the ROBIN fuselage (without a rotor), for which extensive wind tunnel pressure data exist (Ref. 32). The fuselage shape is mathematically defined by super-ellipse equations, which are given in Ref. (32). Computations were done for an angle of attack, $\alpha = 0^\circ$ and Reynolds number of 4.5×10^6 . The regular Cartesian grid used for these predictions had $(192 \times 48 \times 56)$ cells, and each of the two computations required 2.5 hrs on a PC (Intel Pentium II, 266MHz).

In general, the surface pressure predictions also agree well with a panel method and "Navier-Stokes" predictions (Ref. 33). By contrast, the panel method cannot treat general separating flows and the "Navier-Stokes" method, for general bodies, requires a lengthy procedure to generate body conforming grids that require very long computational times. We conclude that Vorticity Confinement can serve as the basis of a simple, efficient method for accurately modeling the flow about body surfaces.

4.2.2 Computation of Complete Apache Helicopter in Forward Flight The same overset procedure described in Section 4.1 was used for computing flow over an Apache Helicopter in forward flight. These calculations were performed for an Apache–A helicopter fuselage with a four bladed rotor. The treatment of the body surface was as described in Section 3.3. Two computational cases, ascending and level forward flight, are presented. These solutions were also presented in Ref. (30). The level flight solution illustrates the vortex merging property of the basic method. The (inner) blade fitted C-grid had 120x26x24 cells and the background Cartesian grid had 162x108x54 cells. The computation required 2.5 hrs/revolution on a CRAY YMP.

The tip vortices are visualized by the iso-surface of vorticity magnitude in Figures 1-4. In these pictures, the contour level of vorticity magnitude is set to 30% of the maximum vorticity magnitude. A short movie which shows the developing of the tip vortices can be viewed at www.flowanalysis.com.

4.2.3 Circular Cylinder The computation of flow around a circular cylinder has been done using both the Vorticity Confinement method presented here (VC1) and a newer formulation (VC2). Reynolds number was 3,900 in both cases. A coarse, uniform Cartesian grid 181x121x61 was used with an immersed boundary for the cylinder that was only 15 cells in diameter. The results presented here are from the VC2 study, although the VC1 formulation shows no significant difference (results for the VC1 formulation can be found in Ref. (7)). Both VC formulations compared very well with each other and with experiment. VC serves as a very simple way to model Reynolds number effects in this case. Increasing ε smoothly increases instabilities and energizes smaller vortical scales. Values of ε and μ used were 0.325 and 0.15, respectively.

Vorticity magnitude iso-surfaces are shown in Figure 5, where the iso-surface magnitude has a value of 25% of the maximum. Plots corresponding to computed average streamwise velocity along lines behind the cylinder are shown in Figure 6 and RMS streamwise velocity fluctuations are presented in Figure 7. The lines where the measurements were taken are shown in Figure 8. Good agreement with experiment is seen. The pressure distribution on the cylinder surface also compares very well with experiment data, as can be seen in Figure 9. The important point here is that only by adjusting one parameter, ε, which was constant throughout the field, the computed results agreed closely with experiment for all six curves plotted in Figures 6 and 7. Additional comparisons with experiment at different Reynolds number will be required to calibrate the Reynolds number dependence of this parameter. It must be emphasized that the instabilities and chaotic behavior that result when ε is increased are only from three-dimensional effects, as in physical turbulence, and are not due to numerical instabilities: Extensive studies have been done over a much wider range of ε values than that studied here for flows in 2-D, where no instabilities were expected. These only showed stable flow. These studies involved vortices shedding from a two-dimensional cylinder with pairing. Other studies involved isolated, shed wing-tip vortices in three-dimensions.

4.2.4 Comanche Helicopter The flow about a realistic helicopter body (Comanche) was computed. Rotating shanks were included in the computation since they could have a significant effect on the flow behind the pylon. However, the resolution of the

shank geometry should be consistent with that of the vortices which they shed, which are spread over only about 4 grid cells. Accordingly, a simple analytic representation was used for the shanks (as opposed to the main body, which was represented by surface points). The shank and body definitions were then used to compute the geometry—defining level set function for the flow computation.

A simple uniform Cartesian grid was used in the computation, which had 288x64x128 in the streamwise, horizontal and vertical directions, respectively. Figure 10 shows the pressure distribution on the body surface at one time. It can be seen in Figure 11 that strong concentrated vorticity is shed form the pylon. This will cause strong pressure fluctuations on the tail, which is seen in the experiment. In fact, a 5-per-revolution oscillating pressure was computed that corresponded closely to flight test data. Although only 3 revolutions were computed and more are required to get better statistics, good agreement in the comparison of power spectra can be seen in Figure 12. This computation was preformed on a PC (Intel Pentium II, 266 MHz, 256 MB RAM) and required 6 hours per revolution. These Comanche results were initially shown in Refs. (4, 12, 30). The flight test power spectra in Figure 12 are also shown in Ref. (31). (The power spectrum results were computed by Ted Meadowcraft of Boeing, Philadelphia.)

4.3 Blade Vortex Interaction (BVI) The ability of VC to economically simulate propagation of concentrated vortices for BVI has made possible a recent parametric study of two-dimensional BVI cases (Refs. 16, 17). This study also utilized a compressible version of Vorticity Confinement. In these papers, it is also demonstrated that there is excellent agreement between the computations and experiment.

4.4 Lifting Line Representation We are starting a project that involves representing the rotor blades as lifting lines. These do not have a grid associated with them, but move through the Cartesian grid. This is, of course, consistent with the treatment of the shed wake vortices and the body surface. The latter, as explained, is treated as a boundary “immersed” vertical layer that can separate. This treatment of rotors should allow a much faster and simpler computation than the rotor method described in Section 4.1. There, the “TURNS” code had to be coupled to the Cartesian grid and velocities interpolated between the grids, both ways, each time step.

For the lifting line (LL), in a vortex lattice method, the Biot-Savart would, of course be used, based on the current values of the circulation at each span station. This could, perhaps, be implemented here as an additive velocity, but there is a much simpler way:

Since we have a grid on which the equations of motion are solved, the effects of a moving vortical region can be obtained by adding an acceleration (to the grid nodes) near each blade. This would appear as a jet, however, and we believe that the resulting vorticity created would be spread over too large a region if no other terms were employed. However, we have Vorticity Confinement, which is very effective at keeping bound vorticity close to the surface. Hence, we can use the same method to keep the vorticity generated around the current position of the LL confined to the desired, (thin) region. Thus, every time step, the flow velocities must be interpolated to the LL position, and, based on their values, the circulation computed and the added acceleration imposed. There are two possibilities for the circulation, either to use a look-up table, based on separate computations or experiment, or to use a one-way interpolation to a blade-fixed grid near the actual blade, and perform a computation on this “coarse” grid once every number of time steps. This number can be large for computational economy, at least for hover.

4.4.1 Rotor wake computation As a first step, we fix the circulation and examine the ability of Vorticity Confinement to capture the tip vortices which tend to spiral downward. A lightly loaded 2 bladed rotor was simulated with a uniform Cartesian grid of 128x128x128 cells. The computing time was about 3 hours per revolution on a PC (Pentium 4, 2.0 GHz, 1GB RAM). The vortices remained compact, spread over only ~4 grid cells (at the 25% contour vorticity level). The 25% iso-surface is shown in Figure 13 from a perspective and in Figure 14 from a side view. The contour (down to 25% of maximum magnitude) with the computational grid is shown in Figure 15. The contraction and downward motion of the vorticity are about as expected. A set of contour plots, which shows the development of the rotor wake, are shown in Fig. 16.

A very important feature of this computation is the instability, which results in two consecutive spirals eventually wrapping around each other. This is seen in wind tunnel experiments.

Another point concerns numerical issues: As the number of the blades is increased, or the downwash is decreased, (for example, by decreasing the loading), the distance between the spiral turns decreases. There is, of course, a limit where there will not be a sufficient number of gird cells between the turns, and there will be an interaction that is a numerical artifact. The limiting spacing before these

artifacts appear and whether they degrade the accuracy of the computation are being studied.

A rotor wake from a 4 bladed rotor is also presented as shown in Fig. 17. The flow condition and computational setup are the same as the above 2 bladed rotor case. A very interesting result is that the interaction results in a set of disjoint, concentric rings, not quite the spiral of Figure 14. However, this should be a weak effect because the actual spiral angle would be small. In fact, sets of concentric rings have been widely used in the past with the Biot-Savart law as a model for the spiral in vortex filament simulations because they can easily be computed. Quantitative comparison with data is currently being done.

4.4.2 Full Lifting Line Code In parallel to the wake studies, a full code has been developed that uses a separate module to solve for the loading based on the local LL flow, rather than specifying it. This module is currently based on the TURNS code with a body-fitted grid for an actual blade model. It is only used as an input for the loading on the LL, as explained. A convergence history of the loading after a small number of iterations can be seen in Figure 18.

5. Conclusion

The Vorticity Confinement (VC) method has been presented. Although the basic ideas are somewhat different than conventional CFD, there is some commonality with a number of well-known computational methods, such as shock-capturing.

The main goal of VC is to efficiently compute complex high Reynolds number incompressible flows, including blunt bodies with extensive separation and shed vortex filaments that convect over long distances. Almost all of the vortical regions in these flows are turbulent. This means that, for any feasible computation, they must be modeled. The remainder of the flows is irrotational and is defined once the vortical distributions are. Further, these vortical regions are often very thin.

For these reasons, the basic approach of VC is to efficiently model these regions. The most efficient way to do this appears to be to develop model equations directly on the computational grid, rather than to first develop model partial differential equations (pde's) and then attempt to accurately discretize them in these very thin regions.

These goals are easily achieved in the large number of flows where the essential features of the main flow are not sensitive to the internal structure of thin vortical regions. Then, VC can easily be used to capture these regions over only a couple of grid cells and propagate them, essentially as nonlinear solitary waves that "live" on the computational lattice. Flows with these features, that are treatable with the present state of VC, include blunt bodies with separation from edges and other well-defined locations. These configurations include complex geometries that can be easily "immersed" in uniform Cartesian grids using VC. These flows also include vortex filaments which can convect, with no numerical spreading, even over arbitrarily long times, and which can merge automatically with no requirement for special logic. Flows that involve separation from smooth surfaces, and which depend on the turbulent state of the boundary layer, require more detailed modeling, including parameter calibration. This is an area of current investigation.

By contrast, a large amount of effort has been expended over a number of years by a large number of workers to develop and calibrate turbulent pde-based models for conventional eddy viscosity-based CFD schemes, such as RANS and LES. These schemes can be quite complex and can require very fine grids. The important point is that VC, even in its simplest "zeroth order" form with constant coefficients, on a coarse grid, can capture most of the main features of high Reynolds number flows. This is mainly because VC involves, in addition to a positive eddy-type viscosity, a negative one that does not diverge, but automatically saturates. This allows a much simpler turbulence modeling approach. Further, arguments (presented in Ref. (14)) show that just such a negative viscosity should be required: Even with no numerical dissipation issues, to accurately simulate a filtered field, in certain regions of the flow, a term should be added to the Euler equations that acts like such a negative dissipation with saturation.

Preliminary results, some of which are presented, suggest that very large computer savings can be achieved, even with the simplest form of VC.

6. Acknowledgements

Development of the method and the work presented here were partially supported by the Army Research Office, the Army Aeroflightdynamics Directorate, NASA and Army SBIR grants, and the University of Tennessee Space Institute (UTSI). Meng Fan of UTSI did the computation of flow around the circular cylinder. Lesong Wang assisted in the preparation of the paper.

7. References

1. Steinhoff, J., and Underhill, D., "Modification of the Euler equations for vorticity confinement application to the computation of interacting vortex rings", *Physics of Fluids*, 6, 1994. pp.2738-2743.

2. Steinhoff, J., Puskas, E., Babu, S., Wenren, Y., and Underhill, D., "Computation of Thin Features over Long Distances Using Solitary Waves", Proceedings of AIAA 13th Computational Fluid Dynamics Conference, July 1997. pp.743-759.
3. Steinhoff, J., Wang, Clin, Underhill, D., Mersch, T. and Wenren, Y., "Computational Vorticity Confinement: A Non-Diffusive Eulerian Method for Vortex-Dominated Flows", UTSI Preprint, 1992.
4. Steinhoff, J., "Vorticity Confinement: A New Technique for Computing Vortex Dominated Flows", *In Frontiers of Computational Fluid Dynamics* (Caughey, D. and Hafez, M., eds), John Wiley & Sons, 1994. pp.235-264.
5. Pevchin, S.V., Steinhoff, J., and Grossman, B., "Capture of Contact Discontinuities and Shock Waves Using a Discontinuity Confinement Procedure", AIAA Paper 97-0874, 1997.
6. Steinhoff, J., Mersch, T., and Wenren, Y., "Computational Vorticity Confinement: Two Dimensional Incompressible Flow", Proceedings of the sixteenth Southeastern Conference on Theoretical and Applied Mechanics, 1992. pp.III.II.73-III.II.82.
7. Fan, M., Wenren, Y., Dietz, W., Xiao, M., and Steinhoff, J., "Computing Blunt Body Flows on Coarse Grids Using Vorticity Confinement", *Journal of Fluids Engineering*, 124, No. 4, pp.876-885, December 2002.
8. Underhill, D. "Investigation of the Vorticity Confinement Method for Flows with Separation", PhD Dissertation, University of Tennessee Space Institute, May, 1997.
9. Steinhoff, J., Wenren, Y. and Wang, L., "Efficient Computation of Separating High Reynolds Number Incompressible Flows Using Vorticity Confinement", AIAA-99-3316-CP, 1999.
10. Steinhoff, J.,et.al, "Vorticity Confinement: A Survey of Recent Results", Proceedings of 1st Annual ARO Workshop on Vorticity Confinement and Related Methods, UTSI, May 1996.
11. Steinhoff, J., et.al, Proceedings of 2nd Annual ARO Workshop on Vorticity Confinement and Related Methods, UTSI, May 1997.
12. Steinhoff, J., et.al, Proceedings of 3rd Annual ARO Workshop on Vorticity Confinement and Related Methods, UTSI, Nov. 1998.
13. Steinhoff, J., Wenren, Y., Wang, L., Fan, M., Xiao, M., and Braun, C., "Application of Vorticity Confinement to the Prediction of the Wake of Helicopter Rotors and Complex Bodies", *Computational Fluid Dynamics JOURNAL*, Vol. 9, April 2001. Japan.
14. Steinhoff, J., Lynn, N. and L. Wang, "Computation of High Reynolds Number Flows Using Vorticity Confinement: I. Formulation, II. Results," UTSI Preprint, March 2005.
15. Dietz, W., Wenren, Y., Wang, L., Chen, X., and Steinhoff, J., "Scalable Aerodynamics and Coupled Comprehensive Module for the Prediction of Rotorcraft Maneuver Loads," SBIR Final Report, May 2004.
16. Morvant, R., Badcock, K., Barakos, G., and Richards, B., "Aerofoil-Vortex Interaction Simulation Using the Compressible Vorticity Confinement Method," 29th European Rotorcraft Forum, Friedrichshafen, Germany,
September 2003.
17. Morvant, R., "The Investigation of Blade-Vortex Interaction Noise Using Computational Fluid Dynamics," PhD Dissertation, University of Glasgow, United Kingdom, February 2004.
18. Wang, C. Steinhoff, J. and Wenren, Y., "Numerical Vorticity Confinement for Vortex-solid Body Interaction Problems", *AIAA Journal*, Vol. 33, August 1995.
19. Wenren, Y., Fan, M., Wang, L. and Steinhoff, J., "Application of Vorticity Confinement to the Prediction of Flow over Complex Bodies", *AIAA Journal*, Vol. 41, May 2003.
20. Steinhoff, J., Fan, M., Wang, L. and Dietz, W., "Convection of Concentrated Vortices and Passive Scalars as Solitary Waves", *SIAM Journal of Scientific Computing*, Vol. 19, December 2003.
21. Hu, G., Grossman, B. and Steinhoff, J., "A Numerical Method for Vortex Confinement in Compressible Flow", *AIAA Journal*, Vol. 40, October 2002.
22. Costes, M. and Kowani, G., "An Automatic Anti-diffusion Method for Vortical Flows Based on Vorticity Confinement", *Aerospace Science and Technology*, Vol. 7, 2003.
23. Braun, C., "Application of Vorticity Confinement to the Flow over a 6:1 Ellipsoid at High Angles of Attack", Master thesis, Institut fur Luft- und Raumfahrt, RWTH Aachen, Germany, 2000.
24. Steinhoff, J., Fan, M. and Wang, L., "Vorticity Confinement – Recent Results: Turbulent Wake Simulations and a New, Conservative Formulation", *Numerical Simulations of Incompressible Flows*, Ed. By M. M. Hafez, World Scientific, 2003.
25. Hass, S., "Computation of Trailing Vortex Over Long Distances Using Vorticity Confinement", Master thesis, Institut fur Luft- und Raumfahrt, RWTH Aachen, Germany, 2003.
26. Robinson, M., "Application of Vorticity Confinement to Inviscid Missile Force and Moment Prediction", AIAA-2004-0717, AIAA Reno meeting, January 2004.
27. Suttles, T., Landrum, D., Greiner, B. and Robinson, M., "Calibration of Vorticity Confinement

Techniques for Missile Aerodynamics: Part I – Surface Confinement", AIAA-2004-0719, AIAA Reno meeting, January 2004.
28. Caradonna, F.X., and Tung, C. "Experimental and analytical studies of a model helicopter in hover." Technical report, NASA TM-81232, 1981.
29. Srinivasan, G.R., Baeder, J.D., Obayashi, S. and McCroskey, W.J. "Flowfield of Lifting Rotor in Hover: A Navier-Stock Simulation." *AIAA Journal*, 30(10): 2371-2378,Oct,1992.
30. Wenren, Y. and Steinhoff, J., "Application of Vorticity Confinement to the Prediction of the Wake of Helicopter Rotors and Complex Bodies", AIAA-99-3200, 17th Applied Aerodynamics Conference, July 1999.
31. Duque, E. and Meadowcraft, E., "Numerical Evaluation of Main Rotor Pylon Flowfields on the RAH-66 Comanche Helicopter," in Proceedings, the AHS 55 th Annual Forum and Technology Display, May 1999.
32. Freeman, C.E. and Mineck, R.E., "Fuselage Surface Pressure Measurements of a Helicopter Wind Tunnel Model with a 3.15-Meter Diameter Single Rotor", NASA TM-80051, March 1979.
33. Chaffin, M.S. and Berry, J.D., "Navier-Stokes and Potential Theory Solutions for a Helicopter Fuselage and Comparison with Experiment", NASA TM-4566, 1994.

8. Figures

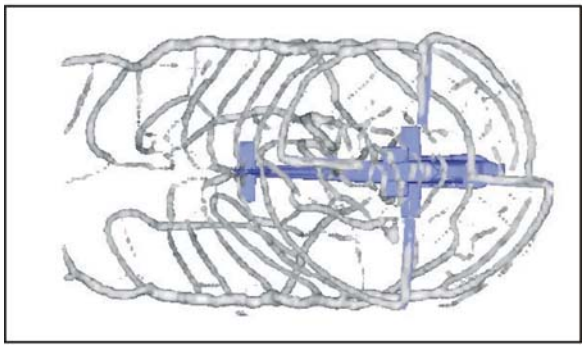

Figure 1. Top view of the computed vorticity iso-surfaces for the Apache helicopter.

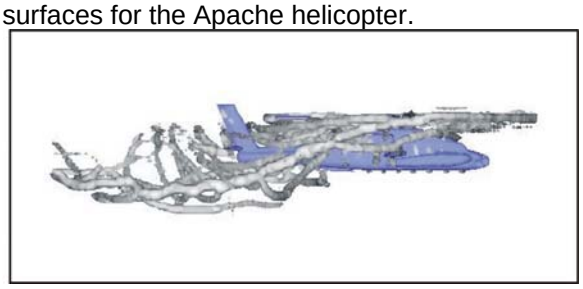

Figure 2. Side view of the computed vorticity iso-surfaces for the Apache helicopter.

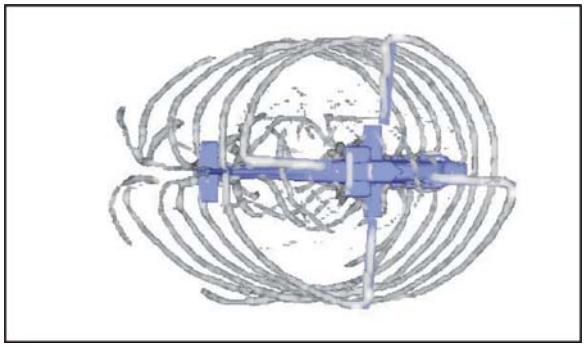

Figure 3. Top view of the computed vorticity iso-surfaces for the Apache helicopter.

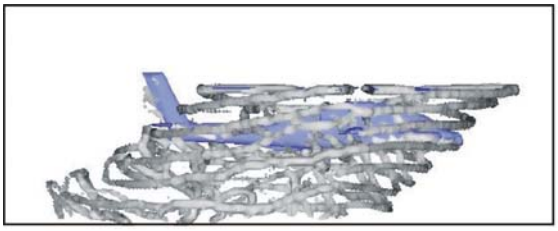

Figure 4. Side view of the computed vorticity iso-surfaces for the Apache helicopter.

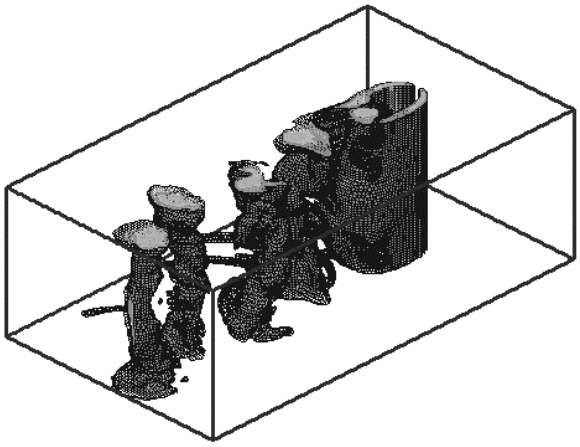

Figure 5. Vorticity Isosurface for Flow over Cylinder with Vorticity Confinement.

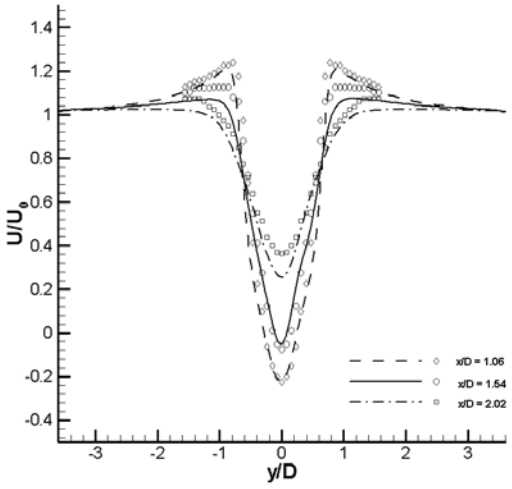

Figure 6. Mean Streamwise Velocity Profiles. Symbols are Experimental Data.

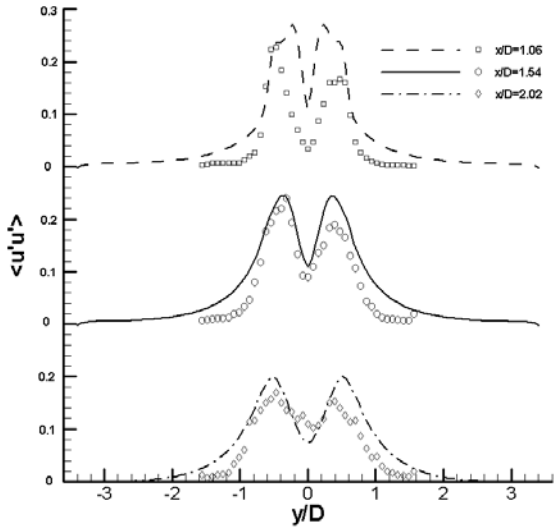

Figure 7. Streamwise RMS fluctuations. Symbols are Experimental Data.

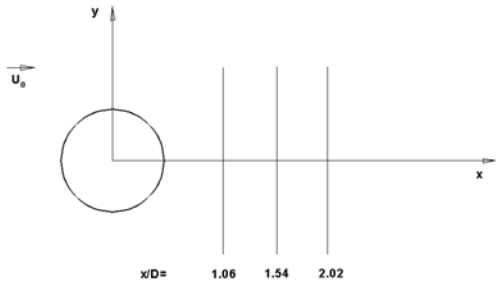

Figure 8. Measurement Positions For Circular Cylinder

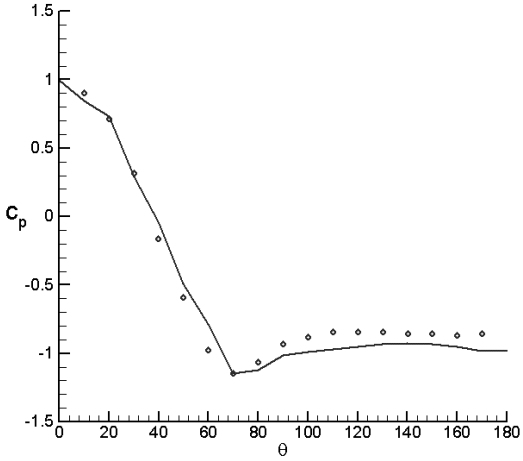

Figure 9. Time-averaged Pressure Coefficient Distribution on the Cylinder Surface. (Circles Denote Experimental Data of Norberg (1987))

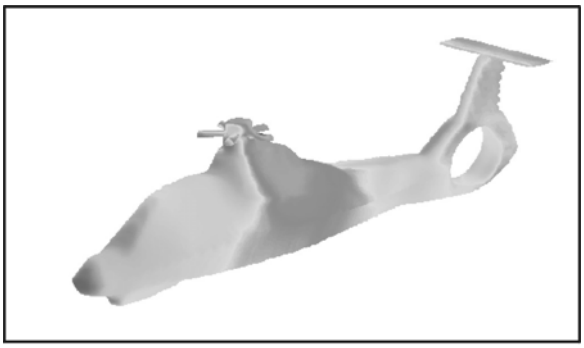

Figure 10. Interpolated surface pressure on the surface of the Comanche fuselage with rotating shanks

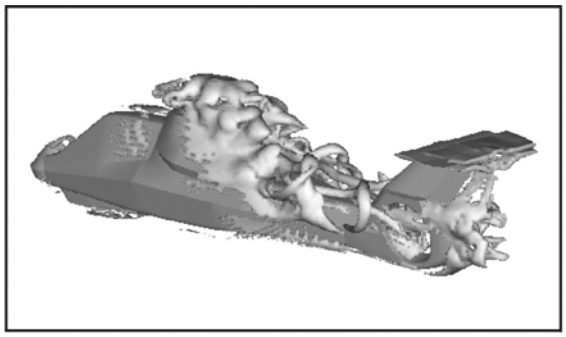

Figure 11. Computed Vorticity Isosurfaces for the Comanche Fuselage with Rotating Shanks

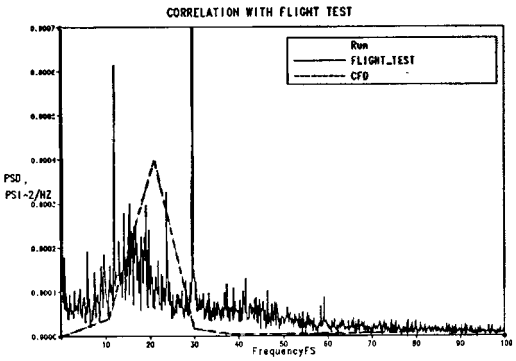

Figure 12. Comparison Between Computation and Flight Test of Power Spectrum of Pressure Fluctuations at Tail

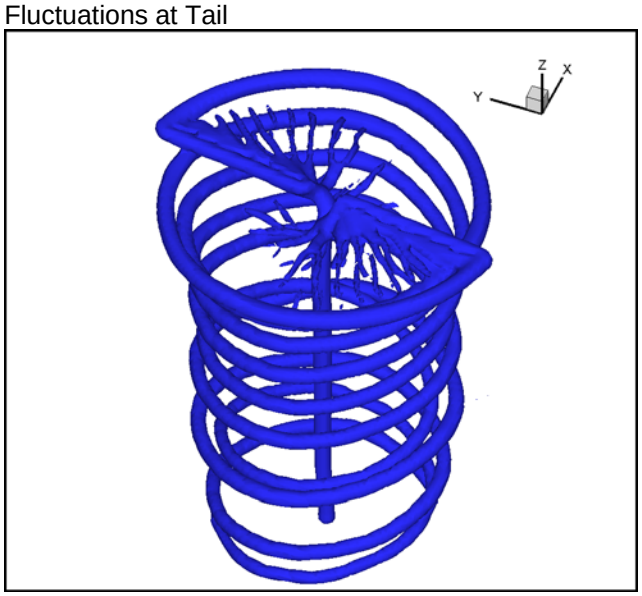

Figure 13. 2-Bladed Rotor Wake Vorticity Isosurface (perspective view)

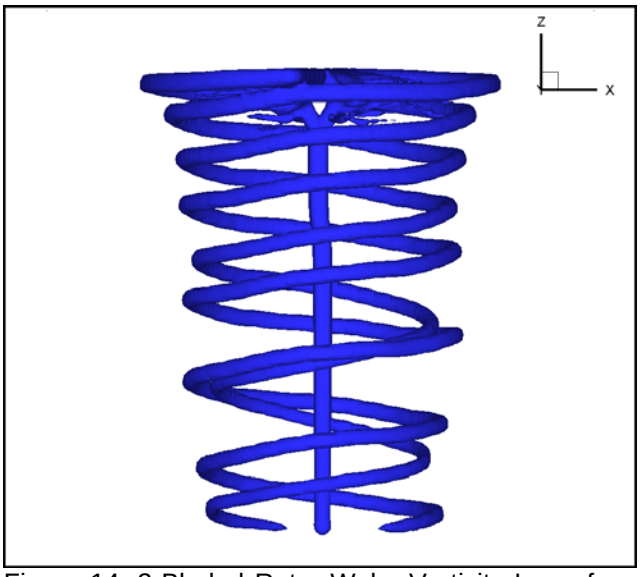

Figure 14. 2-Bladed Rotor Wake Vorticity Isosurface (side view)

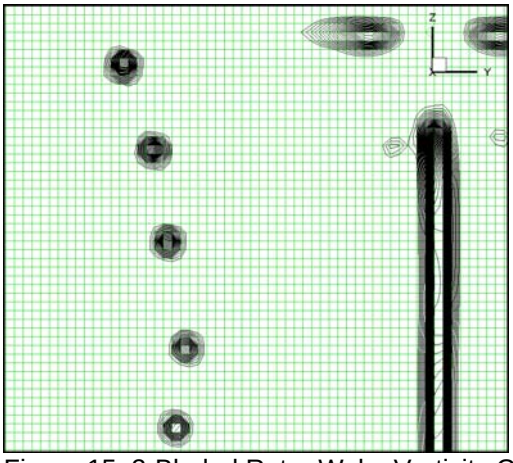

Figure 15. 2-Bladed Rotor Wake Vorticity Contours with Computational Grid

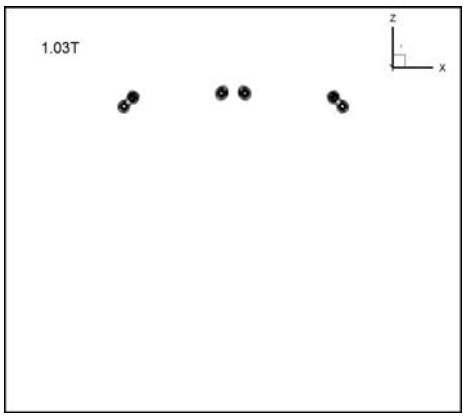

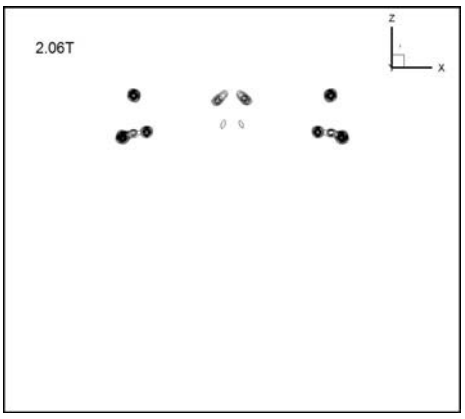

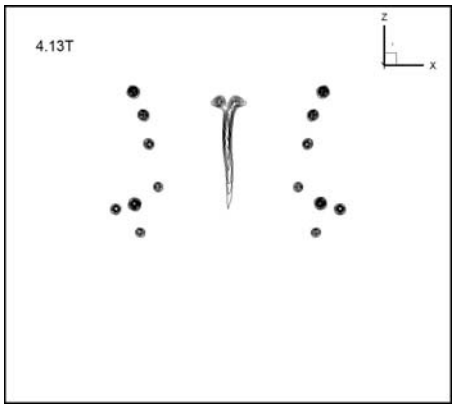
4.13T
z
x

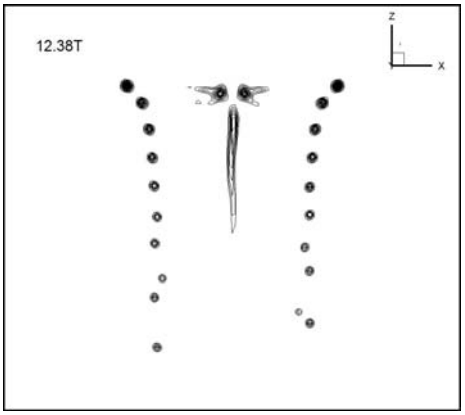
12.38T
z
x

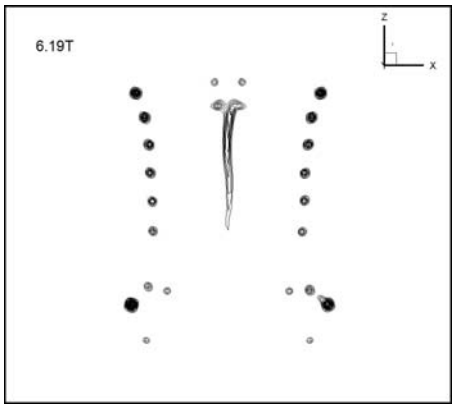
6.19T
z
x

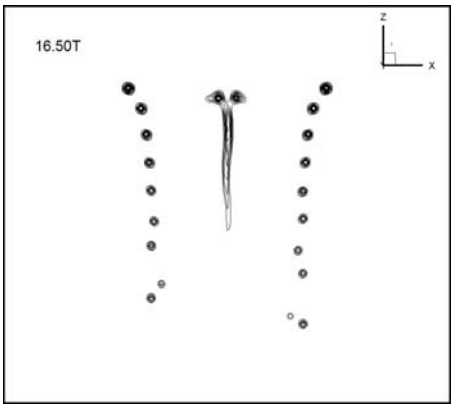
16.50T
z
x

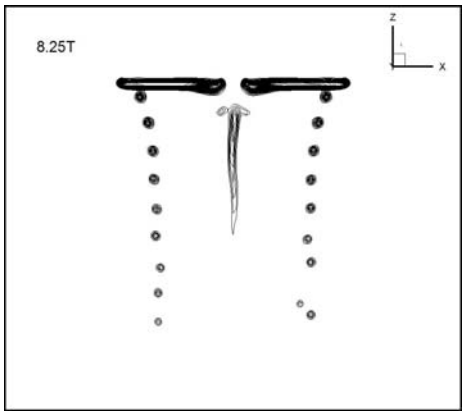
8.25T
z
x

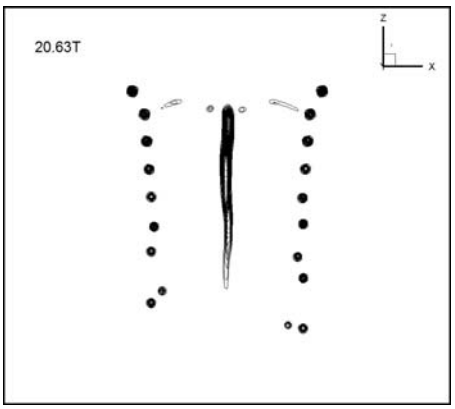
20.63T
z
x

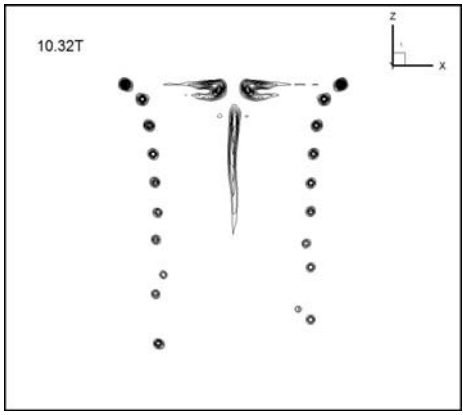
10.32T
z
x

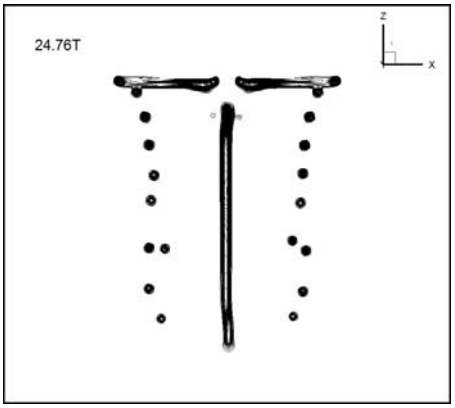
24.76T
z
x

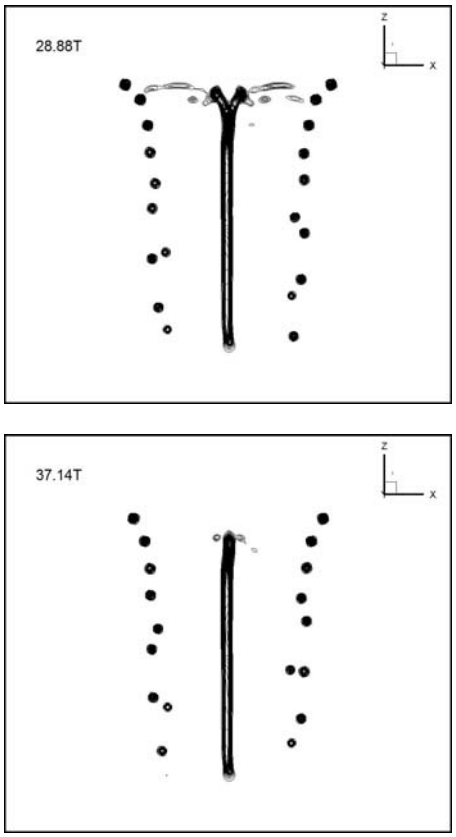

Figure 16. Development of Tip Vortices

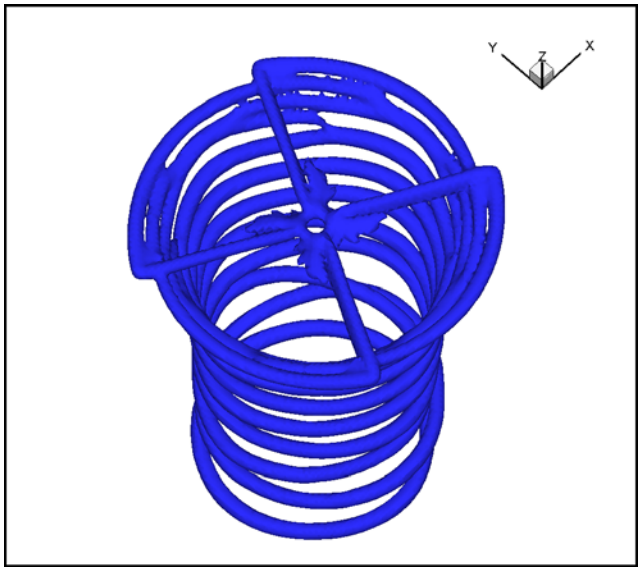

(a) Perspective View

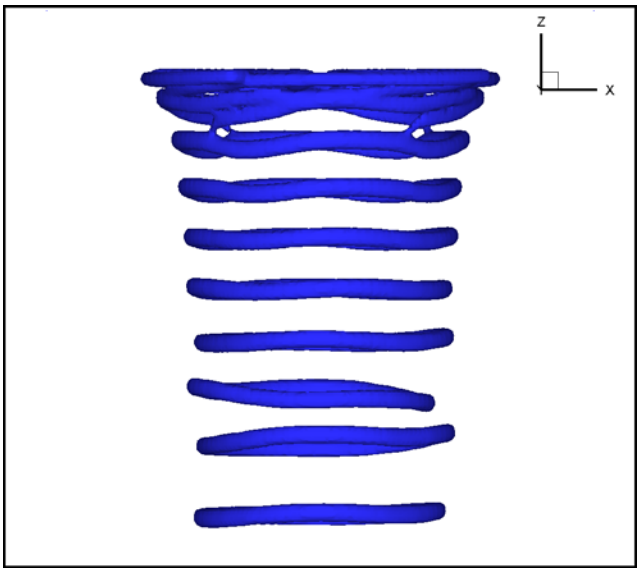

(b) Side View

Figure 17. 4-Bladed Rotor Wake Vorticity Isosurface

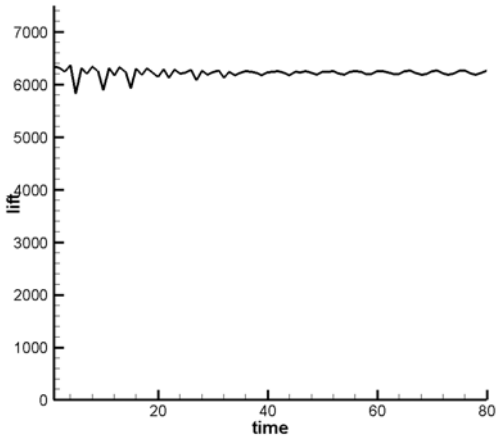

Figure 18. Loading Convergence History Curve